Characterization, pretreatment, and valorization of wood biomass fly ash in a binary cement-free binder

Liang, Xuhui; Dong, Hua; Li, Zhenming; Liu, Chen; Zhang, Shizhe; Ye, Guang

DOI
10.1016/j.dibe.2025.100700

Publication date
2025

Document Version
Final published version

Published in
Developments in the Built Environment

Citation (APA)
Liang, X., Dong, H., Li, Z., Liu, C., Zhang, S., & Ye, G. (2025). Characterization, pretreatment, and valorization of wood biomass fly ash in a binary cement-free binder. *Developments in the Built Environment*, *23*, Article 100700. https://doi.org/10.1016/j.dibe.2025.100700

Developments in the Built Environment 23 (2025) 100700

Contents lists available at ScienceDirect

Developments in the Built Environment

journal homepage: www.sciencedirect.com/journal/developments-in-the-built-environment

Characterization, pretreatment, and valorization of wood biomass fly ash in a binary cement-free binder

Xuhui Liang [a], Hua Dong [a], Zhenming Li [b], Chen Liu [a], Shizhe Zhang [a,c], Guang Ye [a,d,*]

[a] Microlab, Faculty of Civil Engineering and Geoscience, Delft University of Technology, Delft, the Netherlands
[b] School of Civil and Environmental Engineering, Harbin Institute of Technology, Shenzhen, China
[c] Renewi Mineralz & Water Vlasweg 12, PW, Moerdijk, 4782, Rotterdam, the Netherlands
[d] Magnel Laboratory for Concrete Research, Department of Structural Engineering, Ghent University, Ghent, Belgium

ARTICLE INFO

Keywords:
Wood biomass fly ash
Pretreatment
Dissolution
Cement-free binder

ABSTRACT

This research investigated the use of wood biomass fly ash (WBFA) as a key component in developing low-carbon cementitious materials. WBFA was first subjected to water pretreatment and grinding to remove metallic aluminum and free lime, reducing expansion and cracking risks. Characterization of WBFA showed its high calcium and alkali-bearing phases but limited aluminosilicates. Dissolution test showed WBFA had strong alkalinity, suggesting its role as an activator for aluminosilicate-bearing minerals. A novel cement- and chemical-free binary binder was developed using 50 % treated WBFA and 50 % blast furnace slag (BFS). Paste with a water-to-binder ratio of 0.4 achieved 40 MPa compressive strength at 60 days. The use of superplasticizer significantly improved flowability, allowing the water-to-binder ratio to be reduced to 0.25, which resulted in compressive strength up to 58 MPa at 60 days. Calcium aluminate silicate hydrates (C-A-S-H) gels and ettringite were identified as the main reaction products in the pastes.

1. Introduction

The cement industry is estimated to account for about 8 % of global CO_2 emissions, mainly as the result of the high-temperature clinkering process, which involves fuel burning and the decomposition of limestone (Andrew, 2019). The use of Portland cement significantly contributes to the carbon footprint of the construction industry. To mitigate carbon emissions, it is essential to reduce the use of cement clinker. Thus, prevailing methodologies nowadays are either to use supplementary cementitious materials (SCMs) to partially substitute cement clinker, or to develop alternative binders, for instance, alkali-activated materials (AAMs). It is worth noting that the raw materials used as SCMs and in AAMs are primarily derived from industrial by-products, significantly advancing the development of sustainable cementitious materials.

Although a wide range of industrial by-products has been investigated as SCMs or developing AAMs (Ali et al., 2020; Kim et al., 2018; Jiang et al., 2022; Thapa et al., 2019), coal fly ash (CFA), a primary by-product in the coal-fired electricity industry, remains to be one of the most widely used raw material as of now (Yu, 2015; Bentz et al., 2011; Papadakis, 1999; Yan et al., 2024). The standardized quality controls of CFA have resulted in its commercialization as an important raw material in the construction industry. Besides its reduced environmental burden, CFA can also significantly contribute to the performance of cementitious materials in terms of workability, long-term mechanical properties, and durability (Yu, 2015; Chindaprasirt et al., 2004; Bouzoubaâ and Lachemi, 2001; Li and Wu, 2005). Nevertheless, owing to the transitions of the energy industry from fossil fuels to renewable energy sources, coal-fired electricity plants are scheduled to be shut down in the coming years. The coal phase-out action initiated in European countries urges the closure of coal-fired electricity plants by 2030 (Europe Beyond Coal, 2021). Consequently, this has led to a shortage in the supply of CFA in the construction industry. The demand for sustainable cementitious materials necessitates additional sources of raw materials.

Bioenergy, particularly electricity generation from wood biomass combustion, is considered a carbon-neutral source and has been widely accepted by the energy industry (Hektor et al., 2016). Wood bioenergy is nowadays gradually replacing coal-fired electricity plants, showing its prospective development. Similar to CFA, WBFA is the primary by-product produced during the combustion of wood biomass. In 2022, fuel wood consumption in the European Union has reached about 0.72 billion cubic meters (Supply of biomass). Given the ongoing expansion

* Corresponding author. Microlab, Faculty of Civil Engineering and Geoscience, Delft University of Technology, Delft, the Netherlands.
E-mail address: g.ye@tudelft.nl (G. Ye).

https://doi.org/10.1016/j.dibe.2025.100700
Received 9 March 2025; Received in revised form 19 June 2025; Accepted 25 June 2025
Available online 27 June 2025

of wood biomass energy, massive WBFA can be anticipated in the coming years. However, unlike CFA which has been widely accepted in the construction industry, WBFA is currently excluded for cementitious materials according to EN 450–1 (EN 450, 2012). For now, most of WBFA is directly landfilled, leading to a significant financial burden for the energy industry and posing risks for secondary pollution. Therefore, it is of great interest to investigate the feasibility of integrating WBFA into construction practices.

Some research on WBFA has been initiated in recent years. The primary method of WBFA reuse in the construction industry is direct cement replacement, following the approach of conventional SCMs. Through the evaluation of the pozzolanic reactivity, it was found that WBFA presents a less compelling reactivity than conventional SCMs, such as CFA and BFS (Berra et al., 2015; Vu et al., 2019; Teixeira et al., 2019, 2022; Demis et al., 2014). Therefore, the reuse of WBFA is limited. For instance, Rumman et al. (2023) reported that the incorporation of 15, 30, and 45 % of WBFA led to a significant reduction in the 28-day compressive strength by 21, 62, and 71 %, respectively. In another work, only a cement replacement ratio of 5–10 % by WBFA was recommended to ensure cement maintains acceptable long-term strength (Carević et al., 2020). In addition, previous studies on the evaluation of the reactivity of WBFA mainly adopted methods for conventional SCMs such as the Chapelle test (Teixeira et al., 2022) and lime consumption (Rajamma et al., 2009). Given the high availability of calcium sources in WBFA, these methods may lead to an underestimation of the reactivity. Moreover, free lime, which is commonly reported in WBFA (Berra et al., 2015; Maschio et al., 2011; Girón et al., 2013), may pose a threat to the volume stability of cementitious materials. However, this is rarely considered in pretreatment when WBFA is used in blended cement. Owing to the distinct physicochemical properties of WBFA compared to CFA, it is essential to evaluate the potential of WBFA to be recycled in more appropriate methods instead of applying only conventional methodologies of recycling aluminosilicate-bearing minerals.

The aim of this research is to comprehensively analyze the potential of WBFA and its applicability in the development of low-carbon cementitious materials, with the following specific objectives.

1) To apply appropriate pretreatment methods to WBFA to mitigate its expansion risk.
2) To evaluate the feasibility of WBFA in binder formulation.
3) To enhance the use of WBFA in binder systems, exploring the potential in building materials.

In this research, WBFA was first subjected to a pretreatment process to eliminate the potential volume stability threatening factors (i.e., free lime and metallic Al) in cementitious materials. Further, a dissolution test of WBFA in different solutions was conducted to analyze its potential in cementitious materials. Based on the results from the dissolution test, a new WBFA recycling approach was proposed by using treated WBFA as an activator to prepare a chemical- and cement-free binder with tailorable workability and strength.

2. Materials and methods

2.1. Origin of raw materials

WBFA was collected from a bioenergy plant in the Netherlands. The detailed biomass input, combustion devices, burning temperature, and ash collection methods are provided in Table 1.

For comparative purposes, CFA and BFS were introduced as benchmarks alongside WBFA. CFA and BFS were supplied by VLIEGASUNIE B.V. (the Netherlands) and Ecocem B.V. (the Netherlands), respectively.

2.2. Raw materials characterization

The particle size distribution (PSD) of WBFA, as measured by the laser diffraction analyser (Mastersizer, 2000), is shown in Fig. 1. The particle size of WBFA was under 100 μm, a fineness in between that of CFA and BFS, conveying its feasibility to be used as a binder component in cementitious materials from the perspective of PSD.

The chemical compositions of WBFA, CFA, and BFS, determined by the X-ray fluorescence (XRF) technique, are presented in Table 2. Additionally, $WBFA_{mean}$, representing the mean values of the chemical compositions of 97 types of wood biomass fly ash reported in different research, is utilized for comparison with the WBFA in the current research (Liang et al., 2024). In general, WBFA investigated in this research closely resembles $WBFA_{mean}$ in terms of its chemical compositions. This means that the WBFA in the current research can be representative of a broad range of WBFA from the bioenergy industry, making the research results more widely applicable.

WBFA is predominantly composed of calcium, with relatively low amounts of aluminosilicates compared to those with BFS and CFA. The elements associated with pozzolanic reactivity (the sum of silicon, alumina, and iron) only account for 22.81 % of WBFA, considerably lower than the corresponding values in CFA at 87.78 %. These findings suggest a potentially lower pozzolanic reactivity for WBFA. Meanwhile, WBFA is found to have a higher amount of alkali content compared to that in CFA and BFS.

The loss on ignition (LOI) at 1000 °C of WBFA is 6.03 %, within the permitted range for common fly ash used in concrete as required according to EN 450–1 (EN 450, 2012). Moreover, it is important to note that the actual unburnt carbon content in WBFA is only 1.55 %, as determined by the LOI at 550 °C suggested by EN 12880:2000 (NEN-EN 12880, 2001). The continuous mass loss during ignition from 550 °C to 1000 °C is mainly attributed to the decomposition of carbonate-bearing

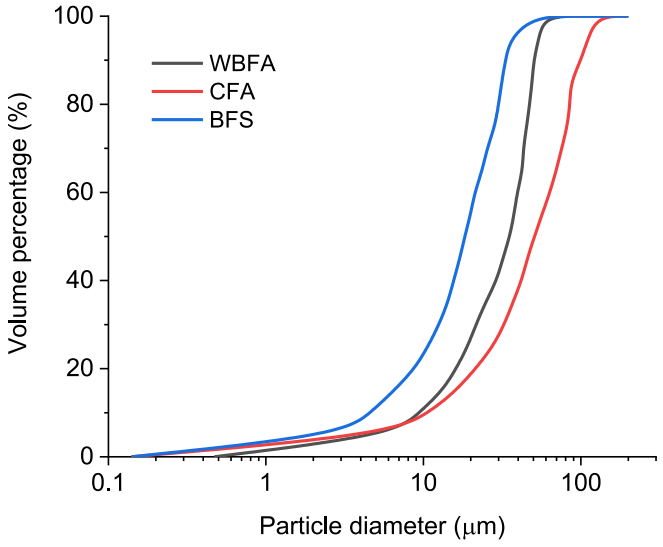

Fig. 1. Particle size distribution of WBFA, BFS, and CFA.

Table 1
WBFA generations parameters.

Biomass type	Burning temperature	Incineration facility	Ash collection method
Wood chips, pruning wood, scrap wood, and paper sludge	900 °C	Bubbling Fluidized bed boiler	Bag filter

Table 2
Chemical compositions (in wt.%) of WBFA, CFA, and BFS determined by XRF.

	SiO_2	Al_2O_3	CaO	Fe_2O_3	SO_3	Na_2O	K_2O	Cl	MgO	LOI (550 °C)	LOI (1000 °C)
WBFA	15.20	4.06	43.65	2.58	6.00	1.77	6.92	3.18	3.33	1.55	6.03
CFA	57.20	24.78	3.96	5.80	0.69	1.28	1.41	–	2.11	1.02	1.27
BFS	31.77	13.25	40.50	0.52	1.49	0.12	0.34	–	9.27	n/a	1.31
$WBFA_{mean}$	21.88	5.19	37.61	2.95	4.44	1.36	10.07	1.69	4.78	n/a	n/a

*n/a: not available.

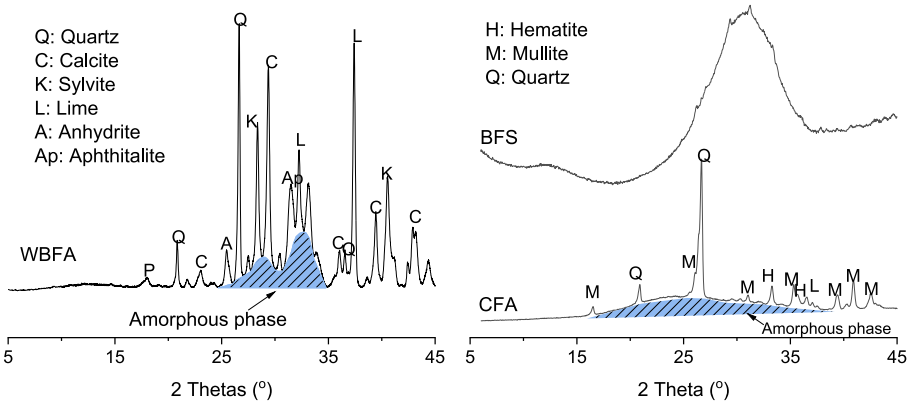

Fig. 2. XRD patterns of raw WBFA, BFS, and CFA.

phases.

The mineral compositions of WBFA were measured by the X-ray diffraction (XRD) technique, and the corresponding patterns are present in Fig. 2. For comparison, the diffraction patterns of BFS and CFA are also present.

The XRD pattern of WBFA is dominated by calcium-bearing phases, including calcite, lime, and anhydrite. Additionally, as WBFA contains a relatively high concentration of alkali, sylvite, aphthitalite, etc., are also observed. Generally, minerals in WBFA are consistent with those frequently reported in previous studies (Vassilev et al., 2013; Gupta et al., 2020). In comparison, minerals present in CFA are quartz, mullite, and hematite, with a minor peak of lime. A clear hump is identified in the pattern between 15 and 35 degrees of 2 thetas, implying the presence of amorphous phases. For BFS, on the other hand, no clear crystalline phase can be identified, and its diffraction pattern is seen as a hump across all diffraction ranges.

The presence of free lime in cementitious materials can pose a potential threat to volume stability, as the slow generation of portlandite with a larger molar volume can lead to expansion in the solid matrix (Min et al., 1996). Since the diffraction peaks of lime are observed in the WBFA pattern, the free lime content was further determined using a titration method according to EN 451–1:2017 (EN 451, 2017). Additionally, the ashes may contain metallic impurities, which could originate from non-separable metal scraps in waste wood products in the manufacturing process (Vassilev et al., 2010). In fact, incineration ash from wastes has often been reported to contain metallic Al (Tian et al., 2020; Segui et al., 2012), which can lead to the generation of hydrogen gas and subsequent cracking in cementitious materials. A setup depicted in Fig. 3 was therefore used to verify the presence of metallic Al in WBFA and to further quantify its amount. For each test, 50 g of WBFA were mixed with 200 ml of a 3 M NaOH solution for 24 h. The suspensions were stirred automatically with a magnetic stirrer to accelerate the metallic oxidation reaction, and the volume of the hydrogen gas was recorded in the graduated cylinder. The metallic Al content in the WBFA was then calculated according to the chemical equation (1), as 1 g of metallic Al could generate approximately 1.25 L of hydrogen gas. Three replicates are conducted for each test.

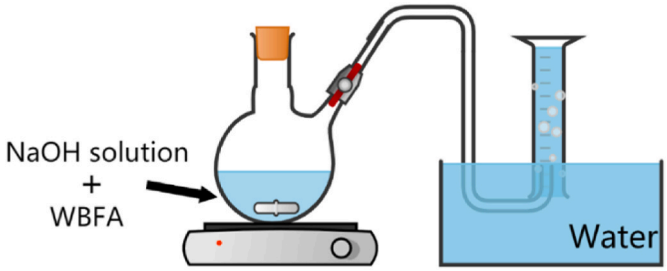

Fig. 3. Schematic diagram of setup for determining metallic Al content.

$$2Al + 2OH^- + 2H_2O = 2AlO_2^- + 3H_2\uparrow \quad (1)$$

Free lime and metallic Al contents are shown in Table 3. The free lime content in fly ash is suggested to be restrained within 1.5 % when used in cement (EN 450, 2012). The high content of free lime in WBFA (8.56 %) is thereby problematic in causing volume expansion. As a result, it is strongly recommended to conduct treatment to reduce the free lime content. On the other hand, WBFA is also found to contain 0.13 % of metallic Al. The presence of metallic Al in WBFA should be strictly prohibited, as a great amount of hydrogen gas can be generated in an alkaline environment. For instance, 1 g of WBFA can already yield approximately 1.63 ml of hydrogen gas. This poses a substantial risk of expansion and cracking in cementitious materials. Therefore, it is suggested to implement a treatment process for the oxidation of metallic Al prior to utilizing the WBFA in cementitious materials.

2.3. WBFA pretreatment

Given that WBFA contains a high content of alkalis and free lime, its inherent alkalinity can be advantageous for eliminating metallic Al. The

Table 3
Metallic Al and free lime content of WBFA.

Free lime (%)	Metallic Al (%)
8.56	0.13

proposed method involved water pretreatment, creating a moist environment to enable the hydration of lime, dissolving alkalis from WBFA, and further facilitating the oxidation of metallic Al by the alkalis (Xuan and Poon, 2018; Huang et al., 2020). To make the pretreatment process more scalable in industrial practices without producing extra wastewater, only a small amount of water was employed to create an earth-moisture state of ash particles, promoting the chemical reaction process.

The overview of pretreatment procedures is summarized in Fig. 4. WBFA was mixed with water at a water-to-ash ratio of 0.2 in a Hobart mixer for 10 min, ensuring complete moistening of the particles. The ash was then sealed and stored in buckets, enabling the reactions to continuously occur. During this period, daily measurements were taken to track the amount of residual metallic Al until its complete oxidation was achieved. Notably, after water pretreatment, particle agglomeration and the formation of hardened coarse particles could be observed, as presented in Fig. 5(b). Therefore, the ash was subjected to grinding to pulverize these particles. It is important to note, that considering the high energy-consuming characteristics of the grinding process, we adopted a tumbling ball milling machine with a low rotation rate (45 rpm) with low energy cost. The treated WBFA underwent testing for its physicochemical properties and was used for further research.

2.4. Treated WBFA characterization

The physicochemical properties of treated WBFA were compared with the raw WBFA. The chemical compositions were determined by XRF analysis. The mineral compositions were measured by XRD. To quantitatively analyze the phase alterations in WBFA after pretreatment, the Rietveld method was employed. For this analysis, 10 % of an internal standard (Si, PDF# 01-086-4266) was homogenously mixed with 90 % ash by weight, and the samples were subjected to an XRD test. The Rietveld analysis was carried out using the BGMN-based program Profex.

The chemical bounds of WBFA before and after pretreatment were compared by using FT-IR (TM 100 Optical ATR-FTIR spectrometer). For each measurement, 20 scans were collected with a resolution of 4 cm^{-1}.

Lastly, the morphology of treated WBFA was investigated by ESEM at a working distance of 10 mm with a voltage of 10 kV (Scrivener et al., 2018)

2.5. Dissolution test

Dissolution is an important process in the hydration of binders. Both crystalline and amorphous phases undergo dissolution in an aqueous solution, releasing ions that contribute to the formation of reaction products. Therefore, a dissolution test was conducted to evaluate the reactive potential of treated WBFA. Three different media, namely deionized water and NaOH solutions with concentrations of 0.1 M and 3 M, were used for the dissolution tests. This allowed the analysing the potential of treated WBFA in terms of its hydraulic properties, pozzolanic activity (with the pore solution at a pH around 13), and/or reactivity for alkaline activation, accordingly.

The treated WBFA was mixed with different media at a mass ratio of 1:100 and horizontally shaken on the shaking table at 200 rpm to prevent precipitation. BFS and CFA were also tested as benchmarks. The suspensions were filtered after a designated period, and the supernatants were collected accordingly. The pH values of these materials were also measured by testing the concentrations of OH^- in the supernatants from water groups by the titration method with 0.1M hydrochloride acid, with phenolphthalein used as the indicator. Subsequently, the supernatants were acidified with nitric acid, diluted, and then subjected to the ion concentration test by Inductively Coupled Plasma Optical Emission spectroscopy (ICP-OES). The concentrations of Ca, Si, and Al were exclusively measured, as these elements are the main components present in the hydration products of cementitious materials.

2.6. Binary binder preparation and performance analysis

The mixture proportions of the binder are provided in Table 4. Paste samples were prepared by using 50 % of treated WBFA and 50 % of BFS as binder components mixed with water. The selected weight ratio of the binder was to achieve approximately 6 % equivalent alkalis content to BSF, which is a typical alkali content in alkali-activated slag. As paste prepared with a water-to-binder ratio at 0.4 (BS_0.4) showed limited flowability, a PCE-based superplasticizer was used to investigate its feasibility in the binder system, aiming for improving the flowability and strength of pastes with reduced lower water-to-binder ratios. Accordingly, BS_0.4, BS_0.3, and BS_0.25 were selected for comparison. A reference mixture, Raw BS_0.4, was prepared using untreated WBFA to measure volume deformation and compressive strength, serving as a comparison to BS_0.4 in order to assess the effectiveness of the WBFA pretreatment.

To prepare the paste, WBFA and BFS were first dry mixed in a Hobart mixer for 5 min to achieve a homogeneous powder. Water was then gradually added, followed by mixing for 3 min at low speed and an additional 1 min at high speed. For pastes containing superplasticizer, superplasticizer was first dissolved in water before being added to the mixer.

The fresh properties of binary pastes were assessed in terms of setting time and flowability. The setting time of pastes was measured accordingly to EN 196-3 (NEN-EN 196, 2016a). The fresh pastes were cast into standard moulds and tested using an automatic Vicat apparatus. During the measurements, the samples were covered with a plastic film to prevent moisture evaporation. The initial setting time was recorded when the needle penetrated to a depth of 35 $\pm$ 3 mm. After the initial setting, the samples were inverted, and the bottom surface was used for the final setting time measurement. The final setting was determined when the penetration depth of the needle was only 0.5 mm. Mini-slump test as illustrated by Li et al. (2021) was used for the flowability measurement. The fresh pastes were cast into a slump cone (with a top inner diameter of 38 mm, bottom inner diameter of 90 mm, and a height of 75 mm) and placed on a glass plate. After filling the cone with paste, it was lifted vertically to allow the paste to flow freely. The flowability was then determined by averaging the lengths measured along two diagonal directions.

The compressive strength of pastes was measured according to EN 196–1 (NEN-EN 196, 2016b). Fresh pastes were cast into cubic moulds with a dimension of 4 cm. After vibration, pastes were sealed with plastic films to avoid moisture loss for 3 days before demoulding.

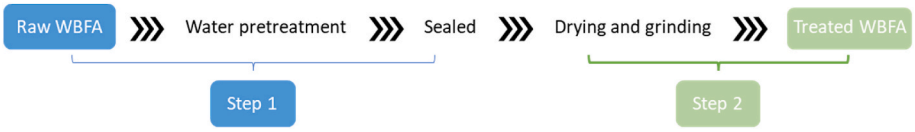

Fig. 4. Flow chart of WBFA pretreatment process.

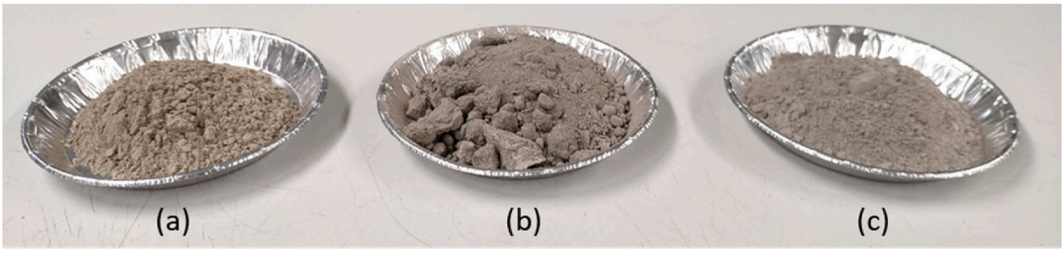

Fig. 5. Appearances of WBFA through pretreatment process
(a: raw WBFA, b: treated ash after step 1, c: treated ash after step 2).

Table 4
Mixture proportions of binary pastes.

Group	Treated WBFA (wt %)	BFS (wt %)	w/b	Superplasticizer (wt % of binder)
Raw BS_0.4	50	50	0.40	0
BS_0.4			0.40	0
BS_0.3			0.30	0.40
BS_0.25			0.25	1.30

Afterward, samples were cured in the curing room at 20 °C and RH above 95 % until the compressive strength test. The loading rate was set to 2.4 kN/s. The average compressive strength of 5 specimens was used as the final strength.

Debris of samples after compressive strength test were collected and subjected to hydration stoppage through solvent exchange, and further used for the measurement of the microstructure. Only mixture BS_0.4 was selected for this measurement to identify the representative microstructure of the binary binder. The test was carried out using ESEM (FEI QUANTA FEG 650) equipped with Energy Dispersive Spectroscopy (EDS), operated at a working distance of 10 mm and a voltage of 10 kV (Scrivener et al., 2018).

The volume deformation of binary pastes was measured according to ASTM C1698-19 (C1698-19, 2019). Fresh pastes were cast into the corrugated tubes with a diameter of 28.5 mm and a length of 425 mm. The length changes of pastes were automatically measured by linear variable differential transformers (LVDTs). The purpose of this measurement is to verify the effectiveness of the pretreatment of WBFA in mitigating the volume expansion caused by metallic Al, thus only Raw BS_0.4 and BS_0.4 were compared.

3. Results and discussion

3.1. Pretreatment of WBFA

To assess the effectiveness of water pretreatment in depleting metallic Al, the changes in residual metallic Al content in WBFA over water pretreatment time were recorded, and the results are illustrated in Fig. 6.

The initial metallic Al content in WBFA is 0.13 %, which decreases to about 0.05 % after 1 day of water pretreatment. Subsequently, the metallic Al depletion rate gradually slows down, taking a total of 6 days to complete its oxidation, reaching 0 %. The observed metallic Al depletion rate generally aligns with the reaction kinetics of metallic Al reported by Xuan et al. (Xuan and Poon, 2018), who introduced alkaline solutions to accelerate the oxidation of metallic Al in municipal solid waste incineration (MSWI) ash. This evidence suggests that the alkalis in WBFA can promote the depletion of metallic Al.

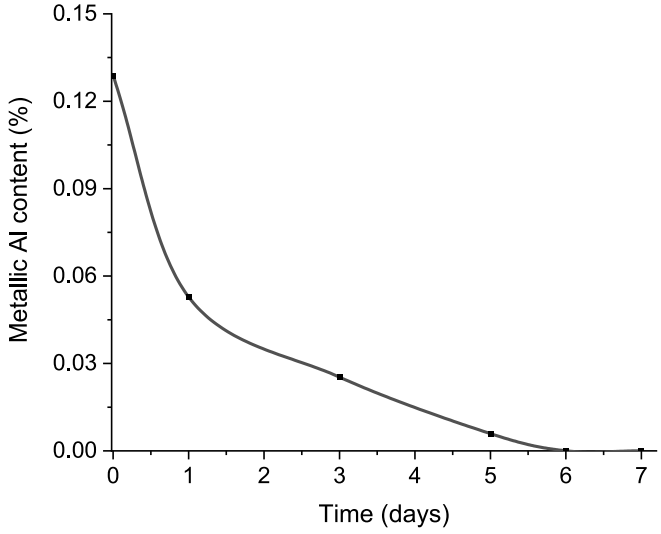

Fig. 6. Correlation between residual metallic Al in WBFA and water pretreatment durations.

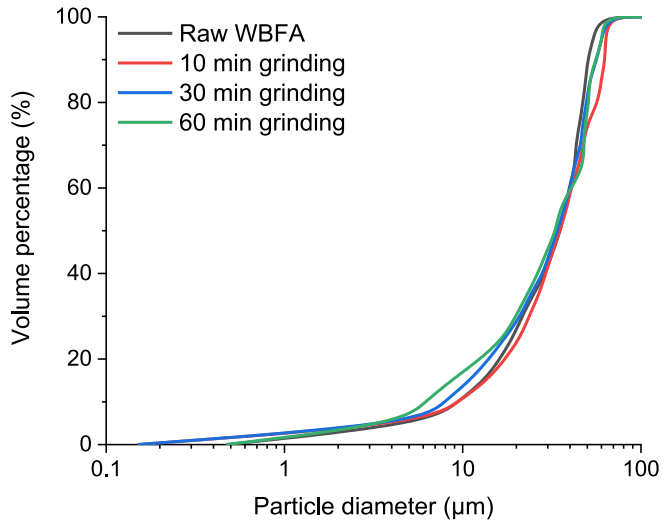

Fig. 7. Particle size distribution of raw WBFA and treated WBFA ground with different durations.

Table 5
Typical particle diameter of raw WBFA and treated WBFA after grinding.

	Raw WBFA	Treated WBFA		
		10 min grinding	30 min grinding	60 min grinding
D10 (μm)	9.41	9.47	7.91	4.61
D50 (μm)	35.33	34.97	34.12	33.25
D90 (μm)	50.26	62.98	56.53	55.74

As indicated in Fig. 5 (b), treated WBFA, after the drying process, exhibits agglomeration and the formation of hardened large particles. The grinding process is therefore necessary to break the agglomeration of water-treated WBFA, ensuring a fine particle size of WBFA that is feasible as a binder component. The effect of grinding durations on the PSD of water-treated WBFA is studied, and the results are presented in Fig. 7 and Table 5. A 10-min grinding process already leads to a fine particle size in the treated WBFA, with D_{10} and D_{50} values reaching 9.47 μm and 34.97 μm, respectively, which is comparable to that of raw WBFA, and can be feasibly used as binder preparation. While longer grinding time could further reduce particle size, it is seen that the size reduction is less significant. As mentioned previously, the motivation for pretreatment is to improve the feasibility of WBFA as a construction material while minimizing costs. Given that grinding is highly energy-demanding, it is therefore recommended to limit the grinding time to 10 min to reduce energy consumption while still achieving effective pretreatment.

3.2. Characteristics of treated WBFA

Water pretreatment not only contributes to the oxidation of metallic Al, but other chemical reactions involving multiple phases may also occur simultaneously. Therefore, it is essential to characterize the physicochemical properties of treated WBFA, providing precise information for further study.

3.2.1. Chemical compositions

Table 6 presents the chemical compositions of treated WBFA, with raw WBFA as a comparison. The chemical compositions of treated WBFA remain rather stable in comparison to the raw ash, as the entire process is conducted in a sealed environment, preventing any leaching of elements. Furthermore, there is a marginal increase in LOI, which can only be ascribed to the increased bound water content in the ash after the pretreatment, as a consequence of reactions that occurred during the pretreatment.

3.2.2. Mineral compositions

Fig. 8(a) presents the XRD patterns of WBFA before and after pretreatment. It is seen that quartz and calcite are the two most stable crystalline minerals dominant in both raw and treated WBFA. When comparing WBFA before and after treatment, one notable observation is the disappearance of the diffraction peaks of lime in raw WBFA, while the intensity of the diffraction peaks of portlandite in treated WBFA increases significantly. During the water pretreatment process, lime is hydrated into portlandite (as elaborated in equation (2)) and possibly other calcium-bearing phases. The QXRD results show that the lime content decreases to 0.27 % in treated WBFA. This depletion of lime is particularly favoured, as it suggests that besides metallic Al, the other volume stability-threatening factor in cementitious materials has also been removed.

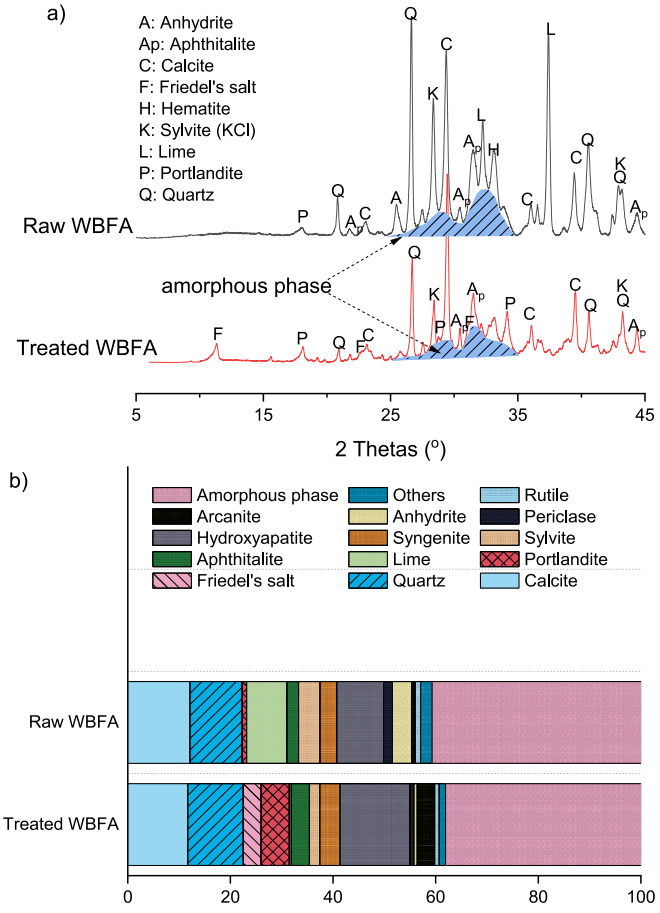

Fig. 8. Comparison of XRD patterns of WBFA before and after pretreatment (a) and their mineral compositions in quantity from QXRD (b).

Furthermore, another new phase, Friedel's salt, is formed after pretreatment. This phase is typically reported in cementitious materials exposed to a chloride-rich environment, such as those serving in marine environments (De Weerdt and Justnes, 2015). The precipitation of Friedel's salt can be elaborated by equation (3), which involves multiple minerals in WBFA including calcium (can be possibly from lime, anhydrite, and portlandite, etc.), sulfate, aluminium (can be possibly from oxidized metallic Al and aluminium-containing glass phases), and chloride (mainly sylvite).

$$CaO + H_2O \rightarrow Ca(OH)_2 \quad (2)$$

$$4Ca^{2+} + 2Al(OH)_4^- + Cl^- + 0.5SO_4^{2-} + 4OH^- + 6H_2O \rightarrow Ca_4Al_2Cl(SO_4)0.5(OH)_{12}\cdot 6H_2O \quad (3)$$

The amorphous contents in raw WBFA and treated WBFA are 40.69 % and 38.06 %, respectively, aligning with previous research indicating a low quantity of amorphous phases in WBFA in the literature(Teixeira et al., 2022; Rumman et al., 2023; Maschowski et al., 2019). Based on

Table 6
Chemical compositions of BFA1 before and after pretreatment.

	SiO_2	Al_2O_3	CaO	Fe_2O_3	SO_3	Na_2O	K_2O	Cl	MgO	LOI 550 °C	LOI 1000 °C
Raw WBFA	15.20	4.06	43.65	2.58	6.00	1.77	6.92	3.18	3.33	1.55	6.03
Treated WBFA	14.98	4.02	41.77	2.32	6.12	1.68	6.53	3.27	2.92	2.67	7.05

Table 7
Chemical compositions of amorphous phase in WBFA before and after pretreatment.

	SiO_2	Al_2O_3	CaO	Fe_2O_3	SO_3	MgO	K_2O	Others	Sum (g/100g ash)
Raw WBFA	5.05	4.06	21.16	0.63	0.81	1.59	0.79	6.60	40.69
Treated WBFA	4.18	3.45	20.86	1.06	0.55	2.18	1.91	3.87	38.06

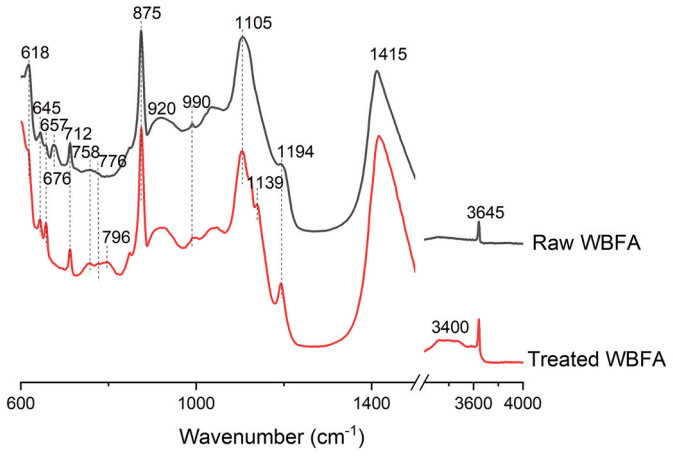

Fig. 9. FT-IR spectra of WBFA before and after pretreatment.

the chemical compositions of quantified crystalline mineral phases from QXRD and the chemical compositions of treated WBFA from XRF, it is possible to obtain the chemical compositions of the amorphous phases in treated WBFA through a mass balance calculation by subtracting the chemical compositions of minerals from bulk raw materials, with results presenting in Table 7.

It is evident that calcium is the dominant element in the amorphous phase of WBFA, which is similar to that reported by Fořt et al. (2024). The chemical compositions of amorphous phases in WBFA remain identical before and after pretreatment, indicating that the primary reactions during pretreatment mainly involve crystalline minerals.

3.2.3. Chemical bonds

The Fourier-transform infrared spectroscopy (FT-IR) technique is used to further investigate the change in chemical bonds of WBFA before and after pretreatment. The corresponding spectra are displayed in Fig. 9, and the main band assignments are listed in Table 8.

The IR bands in WBFA remain almost constant regardless of the pretreatment process. The spectrum of treated WBFA is nearly identical to that of raw WBFA, with three main bands at 875 cm^{-1}, 1105 cm^{-1}, and 1415 cm^{-1}. Specifically, bands at 875 cm^{-1} and 1415 cm^{-1} should be assigned to the bending and stretching of CO_3, respectively (Andersen et al., 1991; McCaslin and White, 2021). Based on the mineral phases, these bands should be attributed to the presence of calcite. The band at 1106 cm^{-1} could be linked to the overlapping of S-O and Si-O bands (Lane, 2007; Kloprogge et al., 2002; Taylor, 1990). Besides, reactive silicate phases with different polymerized degrees are shown in the range of 900–1150 cm^{-1} with several adsorption humps (Taylor, 1990; Zhang et al., 2012, 2017). All this information is well correlated to the previous analysis, showing that WBFA is rich in carbonate, silicate, and sulfate minerals.

By comparing the WBFA before and after pretreatment, a clear difference is the stretching of O-H at 3400 cm^{-1}, which is not clearly observed in raw WBFA but is present in treated WBFA. This band is associated with the chemical water generated during the water pretreatment process (Cheah et al., 2017; Pérez-Villarejo et al., 2018; Wang et al., 2019). In addition, the peak at 3645 cm^{-1}, representative of portlandite (Mollah et al., 2000), shows a significant increase after pretreatment. Such an increase indicates that there is a higher amount of portlandite after pretreatment, which is consistent with the XRD results. A new peak at 796 cm^{-1}, corresponding to the vibration of Al-OH, is seen in the treated WBFA, which should be due to the formation of Friedel's salt (Mollah et al., 2000; Jose et al., 2020). Finally, it is important to note that no C-S-H gel-like phases are formed during the pretreatment of WBFA, as the typical Si-O vibration band for C-S-H gels at 950 cm^{-1} is not observed.

3.2.4. Morphology

The morphology of WBFA before and after pretreatment, measured by SEM, is illustrated in Fig. 10. Unlike CFA particles, which are mainly composed of spherical particles as reported in the literature (Kumar and Kumar, 2011), WBFA particles exhibit mostly irregular shapes. Additionally, some particles still present a fibrous structure, with substances displaying a flocculence texture on the particle surface. Unburnt porous carbons are also clearly visible in the image, consistent with previous findings in the literature (Fořt et al., 2021; Carević et al., 2019).

After pretreatment, the treated WBFA particles exhibit fewer instances of fibrous texture, possibly due to the grinding process that crushes those particles. Moreover, tiny crystals are observed on the surface of most particles, likely the result of the chemical reaction remnants and erosion observed during the pretreatment process.

3.3. Ash dissolution

3.3.1. Dissolution in water

The concentrations of Ca, Si, and Al in the leachates of treated WBFA, BFS, and CFA are plotted as a function of time in Fig. 11. In the leachates of treated WBFA, the concentrations of Ca exhibit a significant increase within the first 30 min, followed by minor fluctuations over the subsequent hours, stabilizing at around 10 mmol/L. It is important to note that the concentrations of Ca in the leachates of treated WBFA consistently surpass those in BFS and CFA at any given time. This can be attributed to the high content of portlandite and the availability of Ca in the amorphous phases of treated WBFA. In the case of CFA leachates, the concentration of Ca experiences a rapid increase within the first 15 min, primarily due to the dissolution of free lime. Once the lime is depleted, the concentration of Ca remains relatively constant. On the other hand, the initial concentration of Ca in BFS leachates is the lowest among the

Table 8
Assignment of the major IR bands in WBFA.

Spectral position (cm^{-1})	Assigned to	Reference
3645	OH (Portlandite)	Mollah et al. (2000)
3400	OH (water molecules)	(Cheah et al., 2017; Pérez-Villarejo et al., 2018; Wang et al., 2019)
712, 875, 1410	CO_3	(Andersen et al., 1991; McCaslin and White, 2021)
618, 657, 676, 1139, 1194	SO_3	(Lane, 2007; Kloprogge et al., 2002)
796	Al-OH	(Cheah et al., 2017; Pérez-Villarejo et al., 2018; Wang et al., 2019)
900–1150	(Si, Al ^{IV})-O-(Si, M), M refers to alkali-earth metals;	(Taylor, 1990; Zhang et al., 2012, 2017)

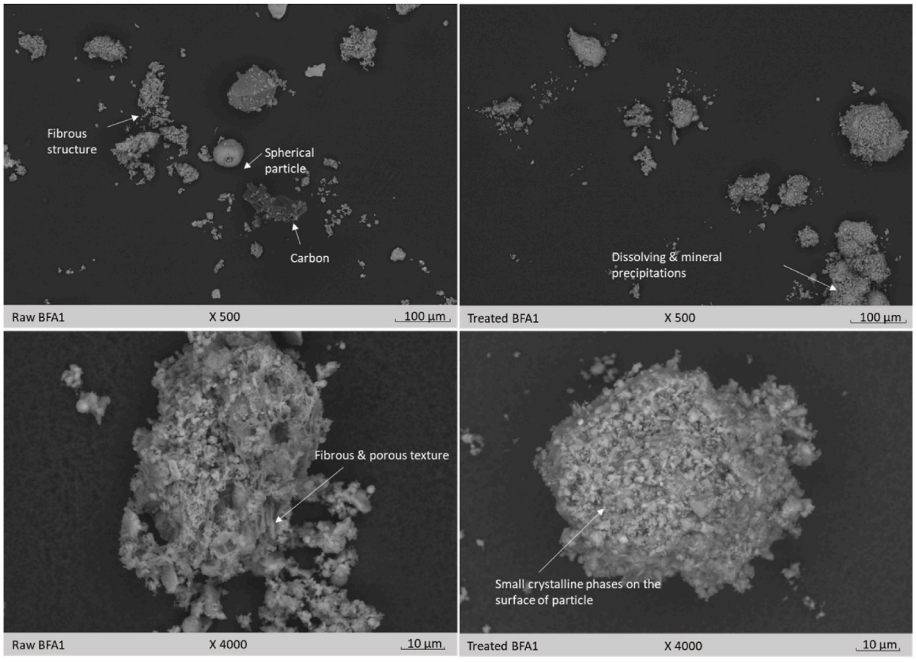

Fig. 10. Morphology of raw WBFA (left) and treated WBFA (right).

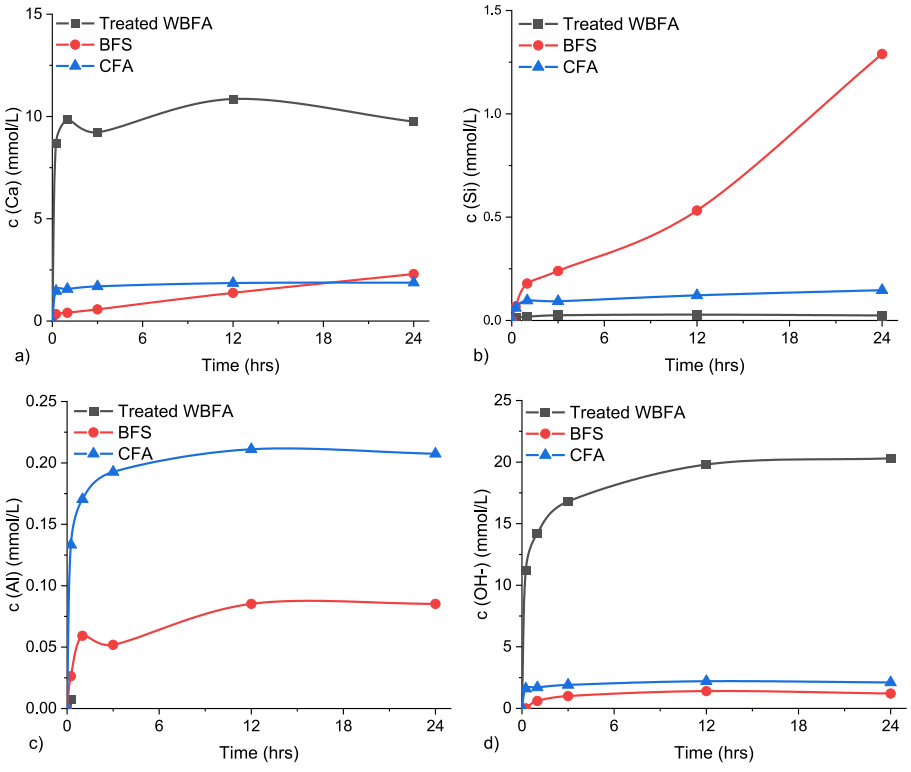

Fig. 11. Dissolution of treated WBFA, BFS, and CFA in deionized water.

three materials. However, it gradually increases over time through a hydrolysis process, facilitated by the dissolution of a substantial amount of Ca from the amorphous phases.

In regard to the dissolution of aluminosilicates, it is found that the concentrations of Si in treated WBFA leachates are plainly low, with a minor increase over time. Furthermore, the concentrations of Al fall below the detection limit. The results are consistent with the limited presence of aluminosilicates in WBFA, as indicated by its chemical compositions. In contrast, in the BFS and CFA leachates, a higher amount of Al and Si can be dissolved compared with those in treated WBFA leachates, as a consequence of the significant presence of amorphous aluminosilicates in these two materials that are more susceptible to dissolve.

Fig. 11(d) illustrates the concentration of hydroxyl ions in leachates during the dissolution process. A small amount of hydroxyl ions can be released from BFS through the hydrolysis process, with a gradual

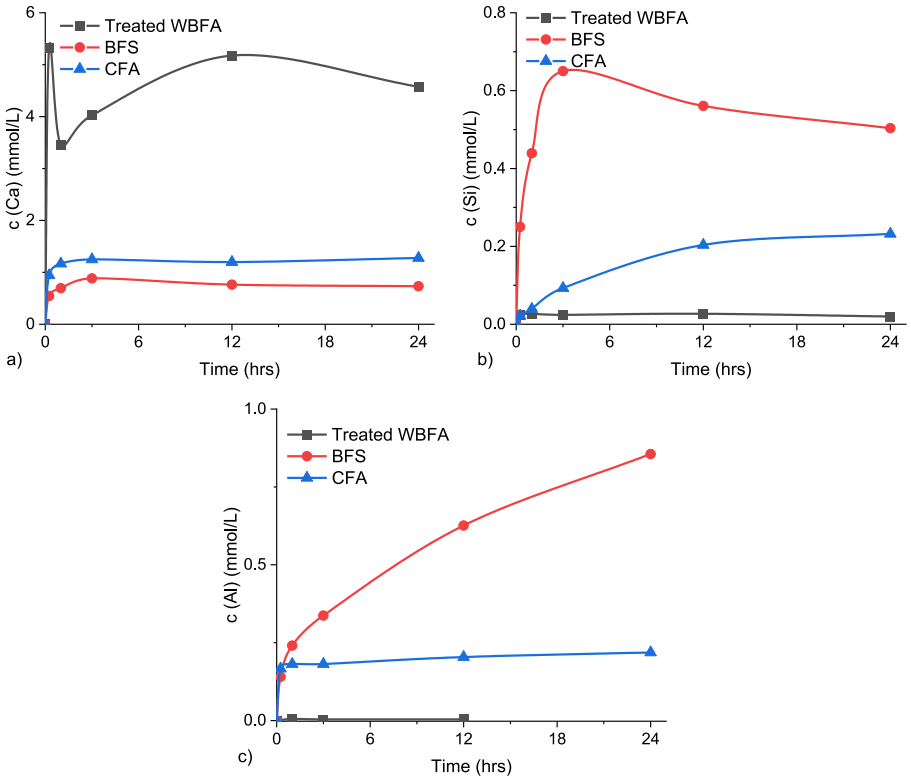

Fig. 12. Dissolution of treated WBFA, BFS and, CFA in 0.1 M NaOH solution.

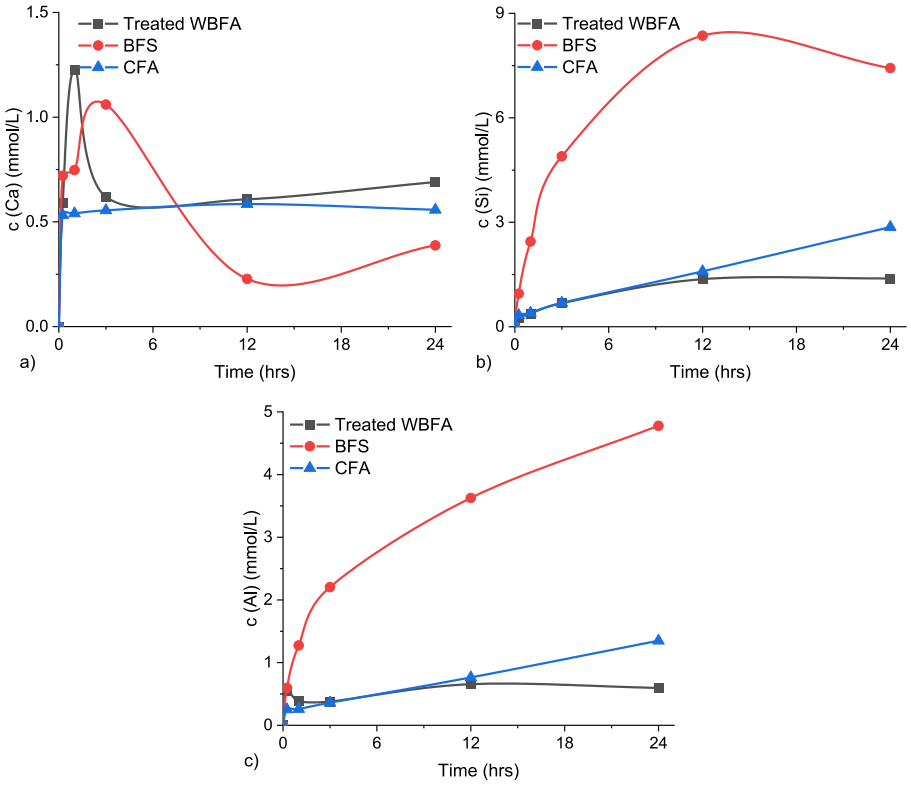

Fig. 13. Dissolution of treated WBFA, BFS, and CFA in 3 M NaOH solution.

increase over time (Dimitrova and Mehanjiev, 2000). The concentration of hydroxyl ions in CFA leachates increases initially in the first 15 min due to the presence of lime, and it remains constant afterward. Notably, the concentration of hydroxyl ions in leachates from treated WBFA is significantly higher than BFS and CFA throughout all stages. This discrepancy can be attributed to the substantial amount of portlandite

and alkaline minerals in treated WBFA. After continuous dissolution for 24 h, the concentration of hydroxyl remains at 20.30 mmol/L in treated WBFA, resulting in a pH value of the leachates at approximately 12.31. The highly alkaline nature of treated WBFA is identified.

3.3.2. Dissolution in alkaline solutions

Figs. 12 and 13 present the concentrations of Ca, Si, and Al in leachates of treated WBFA, BFS, and CFA dissolved from NaOH solutions with molarities of 0.1M and 3M, respectively. With the increment in alkalinity of the solutions, the concentration of Ca in the leachates decreases in all three materials. This can be attributed to the lower equilibrium aqueous solubility of Ca species in solutions with higher alkalinity (Reddy and Subramaniam, 2020). In both 0.1M and 3M NaOH solutions, the concentration of Ca leached from treated WBFA and BFS increases initially and subsequently decreases. This reduction could be ascribed to the precipitates, including portlandite and possibly other Ca-bearing phases (Mikuni et al., 2007). With continuous dissolution, the concentration of Ca would increase further.

The high alkalinity of solutions could promote the initial dissolution of aluminosilicates. As depicted in Fig. 12 (b) (c) and 13 (b) (c), the concentrations of Al and Si in the leachates increase exponentially with the increase in the alkalinity of the solutions. This is in agreement with previous research (Reddy and Subramaniam, 2020; Mikuni et al., 2007; Uvegi et al., 2019). The concentrations of Al and Si dissolved from CFA increase with time in alkaline solutions, while the concentration of Si from BFS is seen with an initial increase followed by a gradual decrease. This should be attributed to the slight precipitations of hydrate phases. Although more Al and Si are dissolved from the treated WBFA in contact with 3M NaOH solution, it should be noted that due to the low content of amorphous aluminosilicates, the concentrations of Al and Si in WBFA leachates are still the lowest among the three materials.

3.3.3. Comments on the potential of treated WBFA in cementitious materials

Considering the characteristics of treated WBFA, its potential as a binder component can be discussed in the following aspects.

1) Self-hardening (latent hydraulic) material.

Self-hardening properties encompass the ability of materials to react with water and solidify with certain mechanical strength. These reactions typically involve the formation of hydrates, such as C-S-H gels, portlandite, and/or ettringite, as reported in previous research (Ohenoja et al., 2016; Illikainen et al., 2014). However, it is unlikely that treated WBFA will exhibit further self-hardening properties, as the limited dissolution of Al and Si from treated WBFA in water suggests that no additional hydrates are expected to precipitate.

2) SCMs in blended cement or precursors in alkali-activation

For both SCMs and precursors, a large content of dissolvable aluminosilicates is demanding. The presence of Al and Si is crucial for promoting the formation of C-(A)-S-H gels in blended cement and calcium-rich geopolymers, or N-A-S-H gels in aluminosilicate-based geopolymers (Garcia-Lodeiro et al., 2011; García-Lodeiro et al., 2010; San Nicolas et al., 2017; Xiao et al., 2020). However, as discussed in previous research (Liang et al., 2024), the majority of WBFA, including the WBFA investigated in the current study, tend to be calcium-rich with limited aluminosilicate content. As indicated by the dissolution tests, when exposed to simulated cement pore solutions (0.1M NaOH), the amount of dissolved Si and Al from treated WBFA is significantly lower than that from BFS and CFA. Although the dissolution of WBFA is enhanced in highly alkaline solutions, such as 3M NaOH, the concentrations of Al and Si remain relatively constant after about 12 h due to the limited amount of dissolvable components. Therefore, the treated WBFA investigated in this research, which is a broad representative of calcium-rich WBFA, seems to be less favourable as a potential source of SCMs or precursors.

3) Minerals with synergistic effect

It is interesting to highlight the high alkalinity of treated WBFA, as well as the large presence of calcium and sulfate-bearing minerals. It is seen that the leachates of treated WBFA in water exhibit a pH value above 12 after 3 h, with a water-to-solid ratio of 100. In binder preparation, a much lower water-to-solid ratio would be applied, thus a higher pH value in the pore solution can be obtained. The high alkalinity from the treated WBFA can be advantageous for the dissolution of aluminosilicate-bearing materials. Moreover, the calcium and sulfate-bearing phases in treated WBFA can also react with aluminate-bearing materials to generate hydrates such as ettringite, monosulfate, etc. In general, these features of WBFA can promote the dissolution of aluminosilicates, leading to the generation of hydrates. Given that neither treated WBFA nor the aluminosilicate-rich mineral alone can lead to a hydration process and obtain mechanical strength, the combining of these two materials can possibly function synergistically in water to form a monolithic solid. A validation of this hypothesis will be conducted in the following Section 4.

4. Performances of treated WBFA-BFS binary binder

Based on the discussions in Section 3.3.3, treated WBFA showing high alkalinity can be advantageous for the reaction of aluminosilicate-rich minerals. For preliminary validation of this hypothesis, a binary binder with WBFA and BFS is developed.

4.1. Workability

As illustrated in Fig. 14(a), BS_0.4 exhibits high viscosity and does not flow once the slump cone is lifted. Unlike conventional alkali-activated slag pastes where the superplasticizer is ineffective, the addition of superplasticizer reduces the water demand for the binary pastes and greatly improves its flowability, as depicted in Fig. 14(b). These results confirm the high adjustability of flowability in binary materials, allowing them to be tailored to meet various construction requirements.

The setting time of pastes can be found in Table 9. While the setting time of the binary paste is much longer than that of Portland cement and waterglass-activated slag, it can still be comparable to those neutral salt-activated slag materials, for instance, sodium carbonate-activated slag (Dai et al., 2023). The long setting time should be mainly attributed to the slow reaction of binders. The solutions should first achieve adequate alkalinity ((pH above 11.5) (Song and Jennings, 1999)) in order to accelerate the dissolution of BFS. The alkalinity of pore solutions, on the other hand, is primarily governed by the dissolution of treated WBFA. These multiple dissolution steps result in a prolonged setting time of pastes.

Furthermore, with the reduction of the water-to-solid ratio, the setting time slightly decreases. This is because a lower water-to-solid ratio may increase the concentrations of [OH] in the aqueous solutions initially, which might facilitate the BFS dissolution. Additionally, by reducing the water-to-solid ratio, the particles are more compacted in the matrix, and the hardness of the paste surface consequently increases. As a result, it becomes more difficult for the Vicat needle to penetrate through the paste.

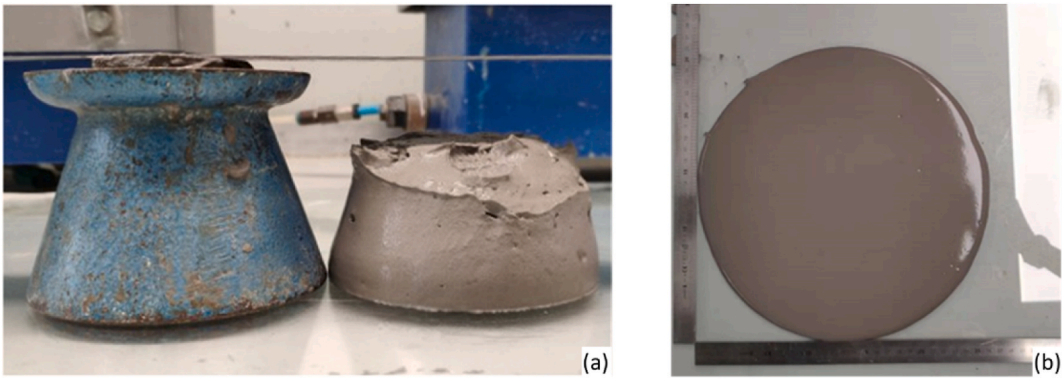

Fig. 14. Mini slump test of BS_0.4 (a) and BS_0.25 (b).

Table 9
Setting time and flowability of the binary pastes with different water to solid ratios.

	BS_0.4	BS_0.3	BS_0.25
Initial setting (min)	610	600	530
Final setting (min)	1215	1170	1030
Flowability (mm)	97	235	271

4.2. Volume deformation

Fig. 15(a) and (b) show the autogenous deformation of binary pastes, with the onset of experiments starting once paste casting. The expansion process caused by metallic Al can be observed in Fig. 15(a). The blending of raw WBFA with BFS results in immediate expansion due to the generation of hydrogen gas, taking approximately 24 h to reach a constant state. Conversely, the binary pastes with treated WBFA and BFS initially undergo shrinkage, which can be attributed to the chemical shrinkage of the pastes (Li et al., 2019). A slight expansion is observed at around 20 h, likely due to the formation of ettringite. The formation of ettringite will be further verified in the subsequent section. A comparison of the cross-sections of the samples in Fig. 15 (c) reveals that the binary pastes containing treated WBFA display a uniform cross-section, while pastes with raw WBFA exhibit heterogeneous expansion and cracks. The pretreatment process effectively mitigates volume expansion-induced cracking caused by metallic Al.

4.3. Compressive strength

As shown in Fig. 16. With a water-to-solid at 0.40, the 7-day compressive strength of paste BS_0.4 can achieve 20 MPa. A continuous increase in strength is found with time, as a result of the continuous generation of hydration products. Comparatively, pastes prepared with raw WBFA showed lower compressive strength, approximately 4 MPa at 7 days and 7 MPa at 60 days. This poor performance of mixture Raw BS_0.4 is primarily attributed to visible cracks caused by metallic Al, which introduced significant defects in the specimens (Fig. 15). These results again highlight the effectiveness of the pretreatment process in enabling the use of WBFA in formulating binders with satisfactory

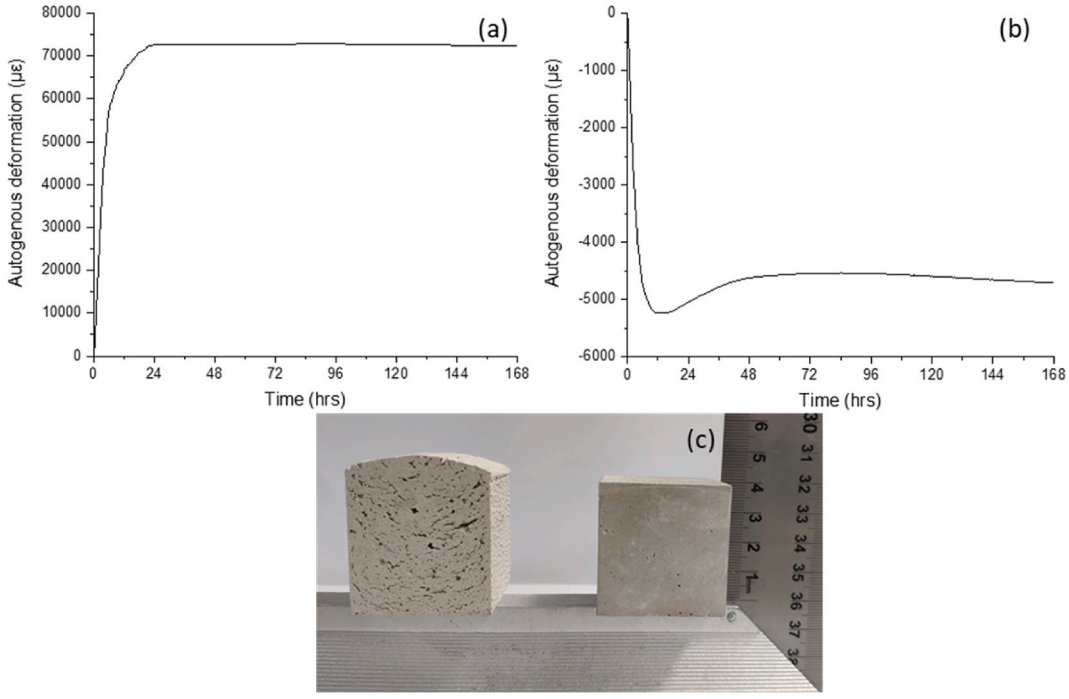

Fig. 15. Deformation of pastes BS_0.4 with WBFA before and after pretreatment
(a: paste with raw WBFA, b: paste with treated WBFA, c: cross-section of the pastes).

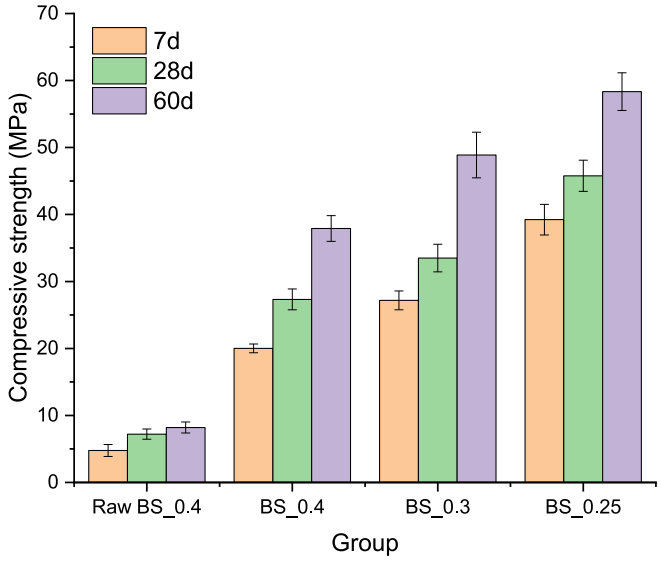

Fig. 16. Compressive strength of binary pastes.

mechanical properties.

By reducing the water-to-solid ratio, it is found that the compressive strength increases accordingly. Pastes are found to achieve the compressive strength of 58 MPa at 60 days. This indicates that the pastes can be tailored for a wide range of applications for strength demand. The strength attained in the binary pastes is comparable to that of alkali-activated slag systems prepared with chemical activators such as sodium sulfate, quicklime, and sodium carbonate (Marsh et al., 2022; Tian et al., 2021; Kang et al., 2025). Notably, no additional chemical activators were used in the binder developed in this study, which highlights the environmental advantages of this binder.

4.4. Micrographs

Fig. 17 presents the micrographs of the fracture surface of binary pastes BS_0.4 at 28 days. As illustrated in the figures, there is the presence of fibrous hydrates that form on the surface of grains, effectively binding the anhydrous particles together as a cohesive structure. Additionally, needle-shaped crystals are observed to fill the pores and contribute to the densification of the overall microstructure of pastes. EDS analysis indicates that the fibrous hydrates can be attributed to the formation of C-A-S-H gels, while the needle-shaped crystals are identified as ettringite. The presence of ettringite also explains the slight expansion of the specimens observed after approximately 20 h.

4.5. Retrospection and prospects on binary pastes

The current work presents investigations into the treatment of WBFA, assessing its potential in cementitious materials with a focus on its functional properties. The treated WBFA was further applied to prepare cement-free binary pastes. This work provided a new solution for WBFA valorization in developing clinker- and chemical-free binders. From the workability perspective, superplasticizer seems to be feasible in improving the flowability and reducing the water-to-binder ratio of paste when needed. The binary pastes achieved moderate compressive strength that is lower than waterglass-activated slag but comparable to those slag pastes activated by neutral salt. Given the successful application of neutral salt-activated slag binders in areas such as concrete and 3D printing, the new WBFA-based binder system might also show strong potential for practical use. This highlights its promise as a sustainable and effective solution for WBFA valorization in both research and industrial contexts. However, further research is required to ensure the safe and reliable use of the WBFA–BFS binary binder. The following aspects are proposed for future investigation.

1) To investigate the fundamental reaction mechanism and kinetics of the binary pastes, thus guiding the mixture designs of the binary with engineered performance.
2) To extend the understanding of the performance and durability of the binary pastes such as shrinkage, carbonation, sulfate attack, alkali

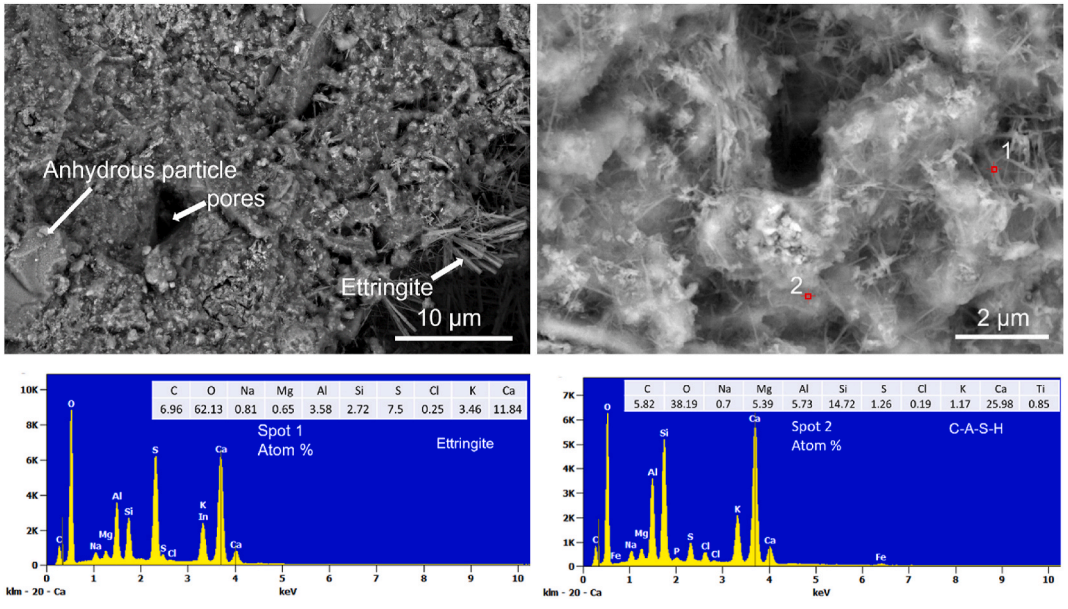

Fig. 17. Micrographs of fracture surface of binary pastes at 28 days.

leaching behaviour, wet-drying, etc., correlating with the microstructure development.

Future research will continue to explore these aspects to advance the knowledge and application of binary binders.

5. Conclusions

In this research, WBFA with representative physicochemical properties was collected and subjected to analysis, pretreatment, characterization, and evaluation of potential recycling approaches. The primary conclusions drawn are as follows.

1) WBFA shows distinct physicochemical properties compared to CFA and BFS. Calcium, silica, potassium, and sulfur are the primary elements of WBFA. From the mineral perspective, the availability of amorphous phases in WBFA was much lower than in CFA and BFS. The presence of metallic Al and free lime in raw WBFA are considered threatening factors that would be detrimental to the volume stability of cementitious materials.
2) The proposed pretreatment process for WBFA involving water pretreatment followed by drying and grinding improves the feasibility of WBFA as a binder component. After 6 days of water pretreatment, metallic Al is fully oxidized, and free lime contents decrease to 0.27 %, effectively eliminating factors that threaten the volume stability of cementitious materials. The subsequent drying and 10-min grinding of water-treated WBFA help to pulverize agglomerated particles, producing fine particles suitable for use as a binder component.
3) The physicochemical properties of treated WBFA are thoroughly analysed with a specific focus on the functional elements, namely Ca, Si, and Al, which are primarily involved in the reaction of cementitious materials and are studied through the dissolution tests. The results show that only limited amounts of Al and Si can be dissolved from treated WBFA, while a high amount of Ca can be extracted. Due to the high availability of calcium and its elevated alkalinity in treated WBFA, it is not recommended to utilize treated WBFA as a conventional SCM. Instead, it is advised to valorise it as a synergetic mineral to enhance the hydration of aluminosilicates.
4) A cement clinker-free paste was developed by combining 50 % of treated WBFA and 50 % of BFS with water. The primary hydrates are C-A-S-H gels and ettringite. This paste is tailorable in terms of flowability with the help of the superplasticizer. The compressive strength of paste at 60 days can be enhanced from 37.91 MPa with a water-to-binder ratio of 0.4 to 58.34 MPa with a water-to-binder ratio of 0.25, indicating its feasibility for different strength demand purposes.

CRediT authorship contribution statement

Xuhui Liang: Writing – original draft, Methodology, Investigation, Formal analysis. **Hua Dong:** Writing – review & editing, Supervision. **Zhenming Li:** Writing – review & editing, Formal analysis. **Chen Liu:** Writing – review & editing, Formal analysis. **Shizhe Zhang:** Writing – review & editing. **Guang Ye:** Writing – review & editing, Supervision, Resources.

Declaration of competing interest

The authors declare that they have no known competing financial interests or personal relationships that could have appeared to influence the work reported in this paper.

Acknowledgement

Xuhui Liang would like to acknowledge the financial supports from the Chinese Scholarship Council (201806050051) and Renewi Mineralz & Water. Zhenming Li would like to acknowledge Guangdong Provincial Key Laboratory of Intelligent and Resilient Structures for Civil Engineering (2023B1212010004).

Appendix

Fig. A1 shows the TGA-DTG curves of WBFA before and after pretreatment. The test was conducted in an argon atmosphere, from 40 °C to 1000 °C with a temperature rising rate of 10 °C/min, aiming to quantify mineral phases such as calcite and portlandite. The consistent results, as shown in Table A2, for portlandite and calcite content from QXRD and TGA indicate good reliability of the QXRD results.

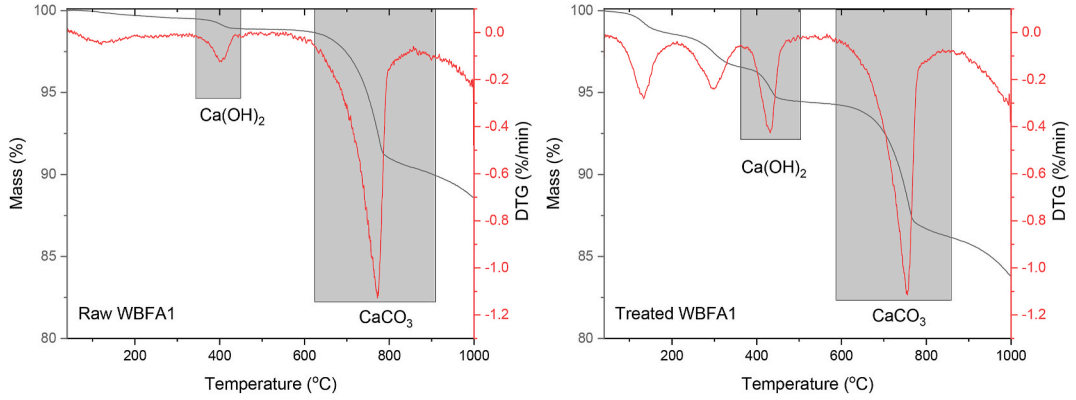

Fig. A1. TGA-DTG curves of WBFA before and after pretreatment.

Table A1
Comparison of the quantifications results (wt. %) of portlandite and calcite in WBFA before and after pre-treatment using TGA and QXRD analysis

	Portlandite		Calcite	
	TGA	QXRD	TGA	QXRD
Raw WBFA	1.12	0.88	12.01	12.13
Treated WBFA	5.92	5.51	11.32	11.7

The reactive silica content of WBFA before and after pretreatment was determined by the dissolution test according to EN 196–2. WBFA was dissolved in dilute hydrochloric acid and further treated in a boiling sodium carbonate solution. The chemical compositions of the insoluble residual can then be determined by the XRF technique, and the reactive silica can be calculated by subtracting the insoluble silica from the total silica content in WBFA. This test was performed to validate the chemical composition of the amorphous phase of treated WBFA calculated by QXRD analysis. In general, the reactive silica content from the dissolution test is similar to, although slightly higher than, the amorphous silica content obtained from QXRD. This difference may arise because, in the dissolution test, WBFA was continuously crushed manually according to the standard EN 196–2, facilitating the dissolution of a small quantity of quartz during the test.

Table A2
Reactive silica content (wt. %) determined by dissolution test according to EN 196-2

Raw WBFA	Treated WBFA
5.97	5.35

Data availability

Data will be made available on request.

References

Ali, H.A., Xuan, D., Poon, C.S., 2020. Assessment of long-term reactivity of initially lowly-reactive solid wastes as supplementary cementitious materials (SCMs). Constr. Build. Mater. 232. https://doi.org/10.1016/j.conbuildmat.2019.117192.

Andersen, F.A., Brečević, L., Beuter, G., Dell'Amico, D.B., Calderazzo, F., Bjerrum, N.J., Underhill, A.E., 1991. Infrared spectra of amorphous and crystalline calcium carbonate. Acta Chem. Scand. 45, 1018–1024. https://doi.org/10.3891/acta.chem.scand.45-1018.

Andrew, R.M., 2019. Global CO2 emissions from cement production, 1928-2018. Earth Syst. Sci. Data 11, 1675–1710. https://doi.org/10.5194/essd-11-1675-2019.

Bentz, D.P., Hansen, A.S., Guynn, J.M., 2011. Optimization of cement and fly ash particle sizes to produce sustainable concretes. Cem. Concr. Compos. 33, 824–831. https://doi.org/10.1016/j.cemconcomp.2011.04.008.

Berra, M., Mangialardi, T., Paolini, A.E., 2015. Reuse of woody biomass fly ash in cement-based materials. Constr. Build. Mater. 76, 286–296. https://doi.org/10.1016/j.conbuildmat.2014.11.052.

Bouzoubaâ, N., Lachemi, M., 2001. Self-compacting concrete incorporating high volumes of class F fly ash: preliminary results. Cem. Concr. Res. 31, 413–420. https://doi.org/10.1016/S0008-8846(00)00504-4.

C1698-19, 2019. Standard Test Method for Autogenous Strain of Cement Paste and Mortar. ASTM. https://doi.org/10.1520/C1698-19.

Carević, I., Serdar, M., Štirmer, N., Ukrainczyk, N., 2019. Preliminary screening of wood biomass ashes for partial resources replacements in cementitious materials. J. Clean. Prod. 229, 1045–1064. https://doi.org/10.1016/j.jclepro.2019.04.321.

Carević, I., Baričević, A., Štirmer, N., Šantek Bajto, J., 2020. Correlation between physical and chemical properties of wood biomass ash and cement composites performances. Constr. Build. Mater. 256, 119450. https://doi.org/10.1016/j.conbuildmat.2020.119450.

Cheah, C.B., Part, W.K., Ramli, M., 2017. The long term engineering properties of cementless building block work containing large volume of wood ash and coal fly ash. Constr. Build. Mater. 143, 522–536. https://doi.org/10.1016/j.conbuildmat.2017.03.162.

Chindaprasirt, P., Homwuttiwong, S., Sirivivatnanon, V., 2004. Influence of fly ash fineness on strength, drying shrinkage and sulfate resistance of blended cement mortar. Cem. Concr. Res. 34, 1087–1092. https://doi.org/10.1016/j.cemconres.2003.11.021.

Dai, X., Ren, Q., Aydin, S., Yardimci, M.Y., De Schutter, G., 2023. Accelerating the reaction process of sodium carbonate-activated slag mixtures with the incorporation of a small addition of sodium hydroxide/sodium silicate. Cem. Concr. Compos. 141, 105118. https://doi.org/10.1016/j.cemconcomp.2023.105118.

De Weerdt, K., Justnes, H., 2015. The effect of sea water on the phase assemblage of hydrated cement paste. Cem. Concr. Compos. 55, 215–222. https://doi.org/10.1016/j.cemconcomp.2014.09.006.

Demis, S., Tapali, J.G., Papadakis, V.G., 2014. An investigation of the effectiveness of the utilization of biomass ashes as pozzolanic materials. Constr. Build. Mater. 68, 291–300. https://doi.org/10.1016/j.conbuildmat.2014.06.071.

Dimitrova, S.V., Mehanjiev, D.R., 2000. Interaction of blast-furnace slag with heavy metal ions in water solutions. Water Res. 34, 1957–1961. https://doi.org/10.1016/S0043-1354(99)00328-0.

EN 450-1, Fly Ash for Concrete - Part 1: Definition, Specifications and Conformity Criteria, 2012.

EN 451-1, Method of Testing Fly Ash - Part 1: Determination of Free Calcium Oxide Content, 2017, p. 1.

Europe Beyond Coal, 2021. Overview: national coal phase-out announcements in Europe. Status January 2021 1–7. https://beyond-coal.eu/wp-content/uploads/2021/01/Overview-of-national-coal-phase-out-announcements-Europe-Beyond-Coal-January-2021.pdf.

Fořt, J., Šál, J., Ševčík, R., Doleželová, M., Keppert, M., Jerman, M., Záleská, M., Stehel, V., Černý, R., 2021. Biomass fly ash as an alternative to coal fly ash in blended cements: functional aspects. Constr. Build. Mater. 271, 71–73. https://doi.org/10.1016/j.conbuildmat.2020.121544.

Fořt, J., Šál, J., Keppert, M., Mildner, M., Hotěk, P., Ślosarczyk, A., Klapiszewski, Ł., Černý, R., 2024. Durability analysis of sustainable mortars with biomass fly ash as high-volume replacement of Portland cement. J. Build. Eng. 91. https://doi.org/10.1016/j.jobe.2024.109565.

García-Lodeiro, I., Fernández-Jiménez, A., Palomo, A., MacPhee, D.E., 2010. Effect of calcium additions on N-A-S-H cementitious gels. J. Am. Ceram. Soc. 93, 1934–1940. https://doi.org/10.1111/j.1551-2916.2010.03668.x.

Garcia-Lodeiro, I., Palomo, A., Fernández-Jiménez, A., MacPhee, D.E., 2011. Compatibility studies between N-A-S-H and C-A-S-H gels. Study in the ternary diagram Na2O-CaO-Al2O3-SiO 2-H2O. Cem. Concr. Res. 41, 923–931. https://doi.org/10.1016/j.cemconres.2011.05.006.

Girón, R.P., Ruiz, B., Fuente, E., Gil, R.R., Suárez-Ruiz, I., 2013. Properties of fly ash from forest biomass combustion. Fuel 114, 71–77. https://doi.org/10.1016/j.fuel.2012.04.042.

Gupta, V., Pathak, D.K., Siddique, S., Kumar, R., Chaudhary, S., 2020. Study on the mineral phase characteristics of various Indian biomass and coal fly ash for its use in masonry construction products. Constr. Build. Mater. 235. https://doi.org/10.1016/j.conbuildmat.2019.117413.

Hektor, B., Backéus, S., Andersson, K., 2016. Carbon balance for wood production from sustainably managed forests. Biomass Bioenergy 93, 1–5. https://doi.org/10.1016/j.biombioe.2016.05.025.

Huang, G., Yang, K., Chen, L., Lu, Z., Sun, Y., Zhang, X., Feng, Y., Ji, Y., Xu, Z., 2020. Use of pretreatment to prevent expansion and foaming in high-performance MSWI bottom ash alkali-activated mortars. Constr. Build. Mater. 245. https://doi.org/10.1016/j.conbuildmat.2020.118471.

Illikainen, M., Tanskanen, P., Kinnunen, P., Körkkö, M., Peltosaari, O., Wigren, V., Österbacka, J., Talling, B., Niinimäki, J., 2014. Reactivity and self-hardening of fly ash from the fluidized bed combustion of wood and peat. Fuel 135, 69–75. https://doi.org/10.1016/j.fuel.2014.06.029.

Jiang, X., Xiao, R., Bai, Y., Huang, B., Ma, Y., 2022. Influence of waste glass powder as a supplementary cementitious material (SCM) on physical and mechanical properties of cement paste under high temperatures. J. Clean. Prod. 340, 130778. https://doi.org/10.1016/j.jclepro.2022.130778.

Jose, A., Nivitha, M.R., Krishnan, J.M., Robinson, R.G., 2020. Characterization of cement stabilized pond ash using FTIR spectroscopy. Constr. Build. Mater. 263. https://doi.org/10.1016/J.CONBUILDMAT.2020.120136.
Kang, X., Tian, Z., Choi, C.E., Ye, H., 2025. Reaction mechanisms of one-part and two-part slag-based binders activated by sodium carbonate and lime. Cem. Concr. Compos. 159, 105992. https://doi.org/10.1016/j.cemconcomp.2025.105992.
Kim, Y., Hanif, A., Usman, M., Munir, M.J., Kazmi, S.M.S., Kim, S., 2018. Slag waste incorporation in high early strength concrete as cement replacement: environmental impact and influence on hydration & durability attributes. J. Clean. Prod. 172, 3056–3065. https://doi.org/10.1016/j.jclepro.2017.11.105.
Kloprogge, J.T., Schuiling, R.D., Ding, Z., Hickey, L., Wharton, D., Frost, R.L., 2002. Vibrational spectroscopic study of syngenite formed during the treatment of liquid manure with sulphuric acid. Vib. Spectrosc. 28, 209–221. https://doi.org/10.1016/S0924-2031(01)00139-4.
Kumar, S., Kumar, R., 2011. Mechanical activation of fly ash: effect on reaction, structure and properties of resulting geopolymer. Ceram. Int. 37, 533–541. https://doi.org/10.1016/j.ceramint.2010.09.038.
Lane, M.D., 2007. Mid-infrared emission spectroscopy of sulfate and sulfate-bearing minerals. Am. Mineral. 92, 1–18. https://doi.org/10.2138/am.2007.2170.
Li, G., Wu, X., 2005. Influence of fly ash and its mean particle size on certain engineering properties of cement composite mortars. Cem. Concr. Res. 35, 1128–1134. https://doi.org/10.1016/j.cemconres.2004.08.014.
Li, Z., Zhang, S., Zuo, Y., Chen, W., Ye, G., 2019. Chemical deformation of metakaolin based geopolymer. Cem. Concr. Res. 120, 108–118. https://doi.org/10.1016/j.cemconres.2019.03.017.
Li, Z., Alfredo Flores Beltran, I., Chen, Y., Šavija, B., Ye, G., 2021. Early-age properties of alkali-activated slag and glass wool paste. https://doi.org/10.1016/J.CONBUILDMAT.2021.123326.
Liang, X., Li, Z., Dong, H., Ye, G., 2024. A review on the characteristics of wood biomass fly ash and their influences on the valorization in cementitious materials. J. Build. Eng. 97, 110927. https://doi.org/10.1016/j.jobe.2024.110927.
Marsh, A.T.M., Yue, Z., Dhandapani, Y., Button, K., Adu-Amankwah, S., Bernal, S.A., 2022. Influence of limestone addition on sodium sulphate activated blast furnace slag cements. Constr. Build. Mater. 360, 129527. https://doi.org/10.1016/j.conbuildmat.2022.129527.
Maschio, S., Tonello, G., Piani, L., Furlani, E., 2011. Fly and bottom ashes from biomass combustion as cement replacing components in mortars production: rheological behaviour of the pastes and materials compression strength. Chemosphere 85, 666–671. https://doi.org/10.1016/j.chemosphere.2011.06.070.
Maschowski, C., Kruspan, P., Garra, P., Talib Arif, A., Trouvé, G., Gieré, R., 2019. Physicochemical and mineralogical characterization of biomass ash from different power plants in the upper rhine region. Fuel 258, 116020. https://doi.org/10.1016/j.fuel.2019.116020.
McCaslin, E.R., White, C.E., 2021. A parametric study of accelerated carbonation in alkali-activated slag. Cem. Concr. Res. 145, 106454. https://doi.org/10.1016/j.cemconres.2021.106454.
Mikuni, A., Komatsu, R., Ikeda, K., 2007. Dissolution properties of some fly ash fillers applying to geopolymeric materials in alkali solution. J. Mater. Sci. 42, 2953–2957. https://doi.org/10.1007/s10853-006-0530-9.
Min, D., Dongwen, H., Xianghui, L., Mingshu, T., 1996. Mechanism of expansion in hardened cement pastes with hard-burnt lime. Cem. Concr. Res. 26, 647–648. https://doi.org/10.1016/0008-8846(96)00021-X.
Mollah, M.Y.A., Yu, W., Schennach, R., Cocke, D.L., 2000. A fourier transform infrared spectroscopic investigation of the early hydration of Portland cement and the influence of sodium lignosulfonate. Cem. Concr. Res. 30, 267–273. https://doi.org/10.1016/S0008-8846(99)00243-4.
NEN-EN 12880, 2001. Characterization of Sludges - Determination of Dry Residue and Water Content, 12880.
NEN-EN 196-3 Methods of Testing Cement - Part 3: Determination of Setting Times and Soundness, 2016.
NEN-EN 196-1 Methods of Testing Cement - Part 1, 2016. Determination of strength.
Ohenoja, K., Tanskanen, P., Wigren, V., Kinnunen, P., Körkkö, M., Peltosaari, O., Österbacka, J., Illikainen, M., 2016. Self-hardening of fly ashes from a bubbling fluidized bed combustion of peat, forest industry residuals, and wastes. Fuel 165, 440–446. https://doi.org/10.1016/j.fuel.2015.10.093.
Papadakis, V.G., 1999. Effect of fly ash on Portland cement systems part I. Low-calcium fly ash. Cem. Concr. Res. 29, 1727–1736. https://doi.org/10.1016/S0008-8846(99)00153-2.
Pérez-Villarejo, L., Bonet-Martínez, E., Eliche-Quesada, D., Sánchez-Soto, P.J., Rincón-López, J.M., Castro-Galiano, E., 2018. Biomass fly ash and aluminium industry slags-based geopolymers. Mater. Lett. 229, 6–12. https://doi.org/10.1016/j.matlet.2018.06.100.
Rajamma, R., Ball, R.J., Tarelho, L.A.C., Allen, G.C., Labrincha, J.A., Ferreira, V.M., 2009. Characterisation and use of biomass fly ash in cement-based materials. J. Hazard. Mater. 172, 1049–1060. https://doi.org/10.1016/j.jhazmat.2009.07.109.
Reddy, K.C., Subramaniam, K.V.L., 2020. Blast furnace slag hydration in an alkaline medium: influence of sodium content and sodium hydroxide molarity. J. Mater. Civ. Eng. 32, 04020371. https://doi.org/10.1061/(asce)mt.1943-5533.0003455.
Rumman, R., Kamal, M.R., Bediwy, A., Alam, M.S., 2023. Partially burnt wood fly ash characterization and its application in low-carbon mortar and concrete. Constr. Build. Mater. 402, 132946. https://doi.org/10.1016/j.conbuildmat.2023.132946.
San Nicolas, R.V.R., Walkley, B., van Deventer, J.S.J., 2017. Fly ash-based geopolymer chemistry and behavior. In: Coal Combust. Prod. Elsevier, pp. 185–214. https://doi.org/10.1016/B978-0-08-100945-1.00007-1.
Scrivener, K., Snellings, R., Lothenbach, B., 2018. A Practical Guide to Microstructural Analysis of Cementitious Materials. CRC Press. https://doi.org/10.1201/b19074.
Segui, P., Aubert, J.E., Husson, B., Measson, M., 2012. Characterization of wastepaper sludge ash for its valorization as a component of hydraulic binders. Appl. Clay Sci. 57, 79–85. https://doi.org/10.1016/J.CLAY.2012.01.007.
Song, S., Jennings, H.M., 1999. Pore solution chemistry of alkali-activated ground granulated blast-furnace slag. Cem. Concr. Res. 29, 159–170. https://doi.org/10.1016/S0008-8846(98)00212-9.
Supply of biomass - annual data, n.d. https://doi.org/10.2908/NRG_CB_BM.
Taylor, W.R., 1990. Application of infrared spectroscopy to studies of silicate glass structure: examples from the melilite glasses and the systems Na2O-SiO2 and Na2O-Al2O3-SiO2. J. Earth Syst. Sci. 99, 99–117. https://doi.org/10.1007/BF02871899.
Teixeira, E.R., Mateus, R., Camões, A., Branco, F.G., 2019. Quality and durability properties and life-cycle assessment of high volume biomass fly ash mortar. Constr. Build. Mater. 197, 195–207. https://doi.org/10.1016/j.conbuildmat.2018.11.173.
Teixeira, E.R., Camões, A., Branco, F.G., 2022. Synergetic effect of biomass fly ash on improvement of high-volume coal fly ash concrete properties. Constr. Build. Mater. 314. https://doi.org/10.1016/j.conbuildmat.2021.125680.
Thapa, V.B., Waldmann, D., Simon, C., 2019. Gravel wash mud, a quarry waste material as supplementary cementitious material (SCM). Cem. Concr. Res. 124, 105833. https://doi.org/10.1016/j.cemconres.2019.105833.
Tian, X., Rao, F., León-Patiño, C.A., Song, S., 2020. Effects of aluminum on the expansion and microstructure of alkali-activated MSWI fly ash-based pastes. Chemosphere 240, 124986. https://doi.org/10.1016/J.CHEMOSPHERE.2019.124986.
Tian, Y., Xing, J., Zhao, Y., Sun, X., Wu, P., Qiu, J., 2021. Influence of aluminum sulfate on strength of CaO-activated slag system. Constr. Build. Mater. 306, 124895. https://doi.org/10.1016/j.conbuildmat.2021.124895.
Uvegi, H., Chaunsali, P., Traynor, B., Olivetti, E., 2019. Reactivity of industrial wastes as measured through ICP-OES: a case study on siliceous Indian biomass ash. J. Am. Ceram. Soc. 102, 7678–7688. https://doi.org/10.1111/JACE.16628.
Vassilev, S.V., Baxter, D., Andersen, L.K., Vassileva, C.G., 2010. An overview of the chemical composition of biomass. Fuel 89, 913–933. https://doi.org/10.1016/j.fuel.2009.10.022.
Vassilev, S.V., Baxter, D., Andersen, L.K., Vassileva, C.G., 2013. An overview of the composition and application of biomass ash. Part 1. Phase-mineral and chemical composition and classification. Fuel 105, 40–76. https://doi.org/10.1016/j.fuel.2012.09.041.
Vu, V.-A., Cloutier, A., Bissonnette, B., Blanchet, P., Duchesne, J., 2019. The effect of wood ash as a partial cement replacement material for making wood-cement panels. Materials 12, 2766. https://doi.org/10.3390/ma12172766.
Wang, X., Ni, W., Jin, R., Liu, B., 2019. Formation of Friedel's salt using steel slag and potash mine brine water. Constr. Build. Mater. 220, 119–127. https://doi.org/10.1016/j.conbuildmat.2019.05.195.
Xiao, R., Jiang, X., Zhang, M., Polaczyk, P., Huang, B., 2020. Analytical investigation of phase assemblages of alkali-activated materials in CaO-SiO2-Al2O3 systems: the management of reaction products and designing of precursors. Mater. Des. 194, 108975. https://doi.org/10.1016/j.matdes.2020.108975.
Xuan, D., Poon, C.S., 2018. Removal of metallic Al and Al/Zn alloys in MSWI bottom ash by alkaline treatment. J. Hazard. Mater. 344, 73–80. https://doi.org/10.1016/j.jhazmat.2017.10.002.
Yan, J., Zhu, Z., Liu, R., Chen, M., Shao, C., Zhang, C., Li, X., 2024. A multi-perspective study on the influence of physical and chemical properties of 5 types of fly ash on the performance of high-volume blended fly ash cementitious slurry. Constr. Build. Mater. 411, 134301. https://doi.org/10.1016/j.conbuildmat.2023.134301.
Yu, Z., 2015. Microstructure development and transport properties of Portland Cement-fly ash binary systems: in view of service life predictions. https://repository.tudelft.nl/islandora/object/uuid:1207b07c-aa48-4992-9bbb-f972e1451a72?collection=research.
Zhang, Z., Wang, H., Provis, J.L., 2012. Quantitative study of the reactivity of fly ash in geopolymerization by ftir. J. Sustain. Cem. Mater. 1, 154–166. https://doi.org/10.1080/21650373.2012.752620.
Zhang, S., Keulen, A., Arbi, K., Ye, G., 2017. Waste glass as partial mineral precursor in alkali-activated slag/fly ash system. Cem. Concr. Res. 102, 29–40. https://doi.org/10.1016/j.cemconres.2017.08.012.